FEBS Letters 582 (2008) 2950–2956

Structural insights into P-glycoprotein (ABCB1) by small angle X-ray scattering and electron crystallography

Christopher A. McDevitt[a], Chitra A. Shintre[b], J. Günter Grossmann[c], Naomi L. Pollock[a], Stephen M. Prince[b], Richard Callaghan[a], Robert C. Ford[b,*]

[a] *Nuffield Department of Clinical Laboratory Sciences, University of Oxford, John Radcliffe Hospital, Oxford OX3 9DU, UK*
[b] *Manchester Interdisciplinary Biocentre, Faculty of Life Sciences, University of Manchester, Manchester M1 7DN, UK*
[c] *Molecular Biophysics Group, School of Biological Sciences, University of Liverpool, Liverpool L69 72B, UK*

Received 23 June 2008; accepted 14 July 2008

Available online 25 July 2008

Edited by Stuart Ferguson

Abstract P-glycoprotein (ABCB1) is an ATP-binding cassette protein that is associated with the acquisition of multi-drug resistance in cancer and the failure of chemotherapy in humans. Structural insights into this protein are described using a combination of small angle X-ray scattering data and cryo-electron crystallography data. We have compared the structures with bacterial homologues, and discuss the development of homology models for P-glycoprotein based on the bacterial Sav1866 structure.

Keywords: Multidrug resistance; Membrane protein; Protein structure; Electron crystallography; SAXS; ABCB1

1. Introduction

The ATP-binding cassette (ABC) family of proteins [1–5] comprise a minimal functional unit of two transmembrane domains (TMDs) and two nucleotide binding domains (NBDs). The TMDs are composed of multiple membrane-spanning α-helices that interact together to form the binding site(s) for the transported allocrite and the translocation pathway across the lipid bilayer. The NBDs power the translocation process via ATP binding, hydrolysis and nucleotide release [1,2]. To date, only low to medium resolution three dimensional structures have been obtained for eukaryotic ABC proteins using electron microscopy (EM) [3,5,6]. Currently, a maximum resolution of ~8 Å [6] has been attained for the nucleotide bound form of mammalian P-glycoprotein (ABCB1) and ~20 Å for the nucleotide free state [7,8]. In contrast high resolution structures of six bacterial ABC transporters have been solved, Sav1866, MsbA, ModBC, BtuCD, $MalFGK_2$ and HI1470/1 [9–16]. However, only Sav1866 and MsbA have been identified as putative exporters, a function shared by eukaryotic ABC transporters. This similarity is supported by amino acid sequence comparisons of eukaryotic ABC proteins with the bacterial ABC proteins for which structural data is available [9–16], with Sav1866 as currently the closest homologue as a basis for homology models.

Recombinant human ABCB1 expressed in insect cell lines has previously yielded highly active protein [17–19], but in insufficient quantities for structural methods such as small angle X-ray scattering (SAXS). Improvements in yield and purity are described herein. SAXS data can be used to provide low resolution models of proteins and protein complexes that are often validated by EM [20,21]. However, SAXS studies can also be used to enhance EM structural data by obtaining a separate measure of the radially averaged amplitude profile [22]. The SAXS data can also correct for the rapid fall-off of amplitudes with resolution with EM data. Noise and errors in EM maps can also be reduced by exploiting any symmetry in the structure. Where symmetry is coincident with a crystal axis (crystallographic symmetry), reciprocal space averaging of the amplitudes is carried out [23]. For other cases, e.g. non-crystallographic symmetry, it is possible to use real-space averaging [24–26].

In this article, we have employed both SAXS and symmetry averaging to improve electron crystallography data for ABCB1 and to help in the interpretation of the resultant density map. This has provided further insights into the ABCB1 map when interpreted in the context of the Sav1866 model.

2. Methods

2.1. Protein expression and purification

The *Trichoplusia ni* (High Five) cell line was maintained in shaking suspension cultures as previously described [17]. Cells at a density of $\sim 3 \times 10^6$ cells ml^{-1} were infected with recombinant baculovirus ($\sim 5 \times 10^7$ plaque-forming units ml^{-1}) at a multiplicity of infection of 10. After 2 h of incubation with virus, the cells were diluted to a density of 1.5×10^6 cells ml^{-1} and grown for a further 3 days before harvesting by centrifugation ($2000 \times g$, 10 min). Crude membrane preparations were isolated as previously described [27], with the exception that buffers contained 20 mM MOPS, pH 7.4, 200 mM NaCl, 0.25 M sucrose. Membranes were solubilised in 20 mM MOPS, pH 7.4, 200 mM NaCl, 1.5 mM $MgCl_2$, 20% glycerol buffer containing 2% (w/v) dodecyl maltoside (DDM) and 0.4% (w/v) lipid (4:1 *Escherichia coli* lipid:cholesterol) and protease inhibitors (Roche, UK) for 60 min at 4 °C and

*Corresponding author. Present address: Molecular Biophysics Group, STFC Daresbury Laboratory, Daresbury Science and Innovation Campus, Warrington, Cheshire WA4 AD, UK. Fax: +44 0161 306 5201.
E-mail address: robert.ford@manchester.ac.uk (R.C. Ford).

Abbreviations: SAXS, small angle X-ray scattering; EM, electron microscopy; ABC, ATP-binding cassette; NBD, nucleotide binding domain; TMD, transmembrane domain; ICL, intracytoplasmic loop; DDM, dodecyl maltoside; SDS–PAGE, sodium dodecyl sulphate–polyacrylamide gel electrophoresis

0014-5793/$34.00
doi:10.1016/j.febslet.2008.07.022

then clarified by ultracentrifugation (100 000 × *g*, 60 min). Supernatants were fractionated using a 5 ml HisTrap column with a stepwise gradient from 40 to 800 mM imidazole. Selected fractions were concentrated using centrifugal ultrafiltration concentrators (Millipore, UK, 100 kDa cut-off). Gel permeation chromatography was performed in 20 mM MOPS, pH 7.4, 200 mM NaCl, 5 mM TCEP, 5% glycerol, 0.02% DDM on a Superdex S200 column 10/30 at a flow rate of 0.3 ml min^{-1}. Protein determination was performed using the BioRad DC Brad protein determination kit with a BSA-calibrated standard curve and with absorbance measured at 750 nm on a Hitachi U200 spectrophotomer. Sodium dodecyl sulphate–polyacrylamide gel electrophoresis (SDS–PAGE) gels were stained using PAGE-Blue (Fermentas, UK).

2.2. SAXS data collection and model generation

SAXS data were recorded at station 2.1 of the Daresbury SRS, UK using a wavelength of 1.54 Å and a sample-to-detector distance of 1 m as described in [28]. Data was collected for a total of 20 min in 60s batches, which allowed for monitoring of any deleterious effects due to exposure to the beam. A similar dataset was collected for the buffer alone and subtraction of the contribution due to buffer was carried out. No change in the scattering profile of neither ABCB1 nor buffer was identified over the data collection period.

Model 3D density distributions were produced ab initio using the GASBOR software [29] which uses simulated annealing to find polymer chain-compatible spatial distributions of dummy residues which fit the experimental SAXS profile. The degree of correspondence between the experimental SAXS data for ABCB1 and the theoretical solution scattering profiles of the density distributions generated by the GASBOR program was good (see Supplementary Fig. 1). The results of 22 GASBOR runs were averaged using the DAMMAVER program [30] to produce a 3D probability map which was then filtered using DAMFILT to a cut-off volume calculated to include the expected protein mass, core glycosylation and detergent.

2.3. Correction of the EM derived map and model fitting

A volume containing one molecule within the ABCB1 EM-derived map was interactively selected using the Chimera software [31], and then pasted into a 120-pixel box for further manipulation using the SPIDER [32] and EMAN [33,34] image processing software suites. The radially averaged structure factor amplitudes were adjusted to match the SAXS amplitude profile (see Fig. 1c) and then applied to the original map [33,34]. The Sav1866 structure [9] (backbone atoms) was initially fitted by hand, and then the local position was refined by using the Chimera 'fit model to map' function. The Fourier shell correlation (FSC) was calculated between the map and a 180° rotated version of it in order to assess the degree of approximation to C2 symmetry. This procedure was repeated after small (2° increment) rotations of the map in order to find the optimal pseudo-C2 symmetry axis, which was within 5° of the initial position.

3. Results and discussion

3.1. ABCB1 purification

Solubilised insect cell membranes were analysed by IMAC (Fig. 1a). Dodeca-histidine tagged ABCB1 eluted at an imidazole concentration of 400 mM. SDS–PAGE indicated that the protein was 80–90% pure. The peak fractions were concentrated and further purified by gel permeation chromatography (Fig. 1b). A peak containing ABCB1 emerged at 12 ml as well as a smaller peak corresponding to the void volume of the column (8 ml) which was due to aggregated ABCB1. The SDS–PAGE analysis indicates that small amounts of ABCB1 are present in this initial aggregation peak. The large peak observed at 18–26 ml corresponds to imidazole. The fractions 11.5–12.5 ml were combined and concentrated to ~5–10 mg ml^{-1} for the SAXS analysis. Dynamic light scattering of the concentrated protein sample (data not shown) confirmed its monodispersity prior to SAXS analysis. Purified, detergent solubilised human P-gp does not display measurable ATPase activity. However, reconstitution of the purified protein, as previously described [18–20], resulted in high rates of drug stimulated ATP hydrolysis (data not shown).

3.2. SAXS data

The SAXS profile for a 6 mg ml^{-1} ABCB1 preparation diluted in the gel permeation chromatography buffer is shown

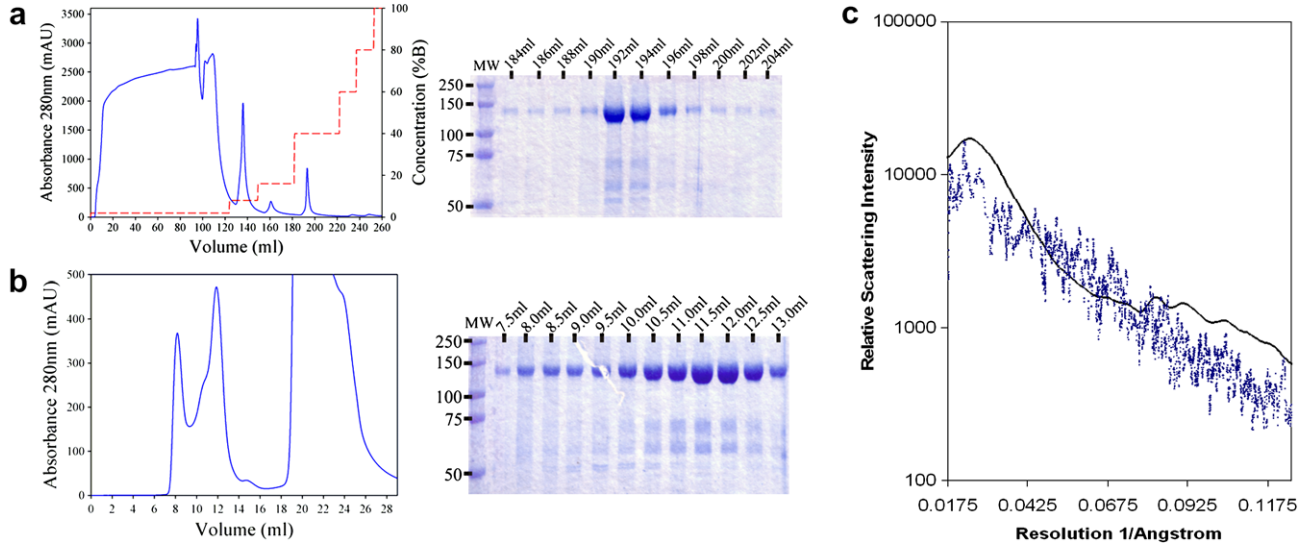

Fig. 1. (a) IMAC purification of dodeca-histidine tagged ABCB1. The solid line is the absorbance at 280 nm and the broken line is the % buffer B (containing 1 M imidazole). SDS–PAGE with PAGE-blue staining of fractions from 184 to 204 ml, corresponding to the main elution peak at 400 mM imidazole, are displayed on the right. (b) Superdex S200 column fractionation of the IMAC-purified ABCB1. The main peak at ~12 ml is preceded by a void volume peak at 8 ml and followed by a large peak corresponding to imidazole (18–26 ml). SDS–PAGE for the indicated fractions is shown on the right. (c) Small angle X-ray scattering (SAXS) profile for DDM-solubilised ABCB1 in the presence of AMP–PNP represented as smoothed fit (solid line) to the measured data. Superimposed (scattered data points) are the EM-derived structure factor amplitudes from 2D crystals of P-gp in the presence of AMP–PNP. For comparison, the two sets of data have been normalised in the middle of the resolution range.

in Fig. 1c. Variations in the low angle scattering region ($s < 0.008$ Å^{-1}) between protein batches were detected and are due to the presence of oligomers (dimers, and higher aggregates) in solution as a result of the protein concentration used. This region of the scattering curve which is associated with intermolecular distances does not affect the EM data adjustment. However, for ab initio generation of density distributions from the SAXS data, a second dataset was recorded for the low angle scattering region at a 10-fold lower protein concentration. The two datasets were then merged to allow a fuller sampling of reciprocal space (see Supplementary Fig. 1). At about $s \approx 0.025$ Å^{-1}, an undulation in the SAXS profile was observed that may be partly due to the presence of a detergent belt surrounding the protein. In contrast, free detergent micelles contribute very little at 0.02% (w/v) DDM – (data not shown). Compared to the SAXS profile, there is some suppression of the low resolution EM amplitudes, probably as a result of the CTF. There is also a more noticeable fall-off of EM-derived amplitudes at higher resolution.

Low resolution density distributions consistent with the SAXS profile of ABCB1 were calculated and the averaged distribution displays a shape approximating a prolate ellipsoid, with overall dimensions of $\sim 150 \times 70 \times 55$ Å (Fig. 2). The maximum diameter D_{max} and the radius of gyration were calculated as 149 and 49 Å, respectively. The unsymmetrised structure has a compact globular region of ~55 Å diameter at the bottom, but has a more open and branched appearance at the top. After orientation along the long axis, C2 symmetry was applied to the density distribution. Automated fitting with the bacterial ABC transporter protein Sav1866 gave an unambiguous alignment of the Sav1866 NBDs with the lower region and its TMDs with the branched upper region. There is a good agreement at very low resolution between the two sets of structural information, but it is difficult to say whether at finer detail, the discrepancies observed in Fig. 2 could be due to real differences between ABCB1 and Sav1866 structures. Ambiguity in the modelling by GASBOR arises mainly because of the absence of the phase component from the SAXS data, but to some extent this is overcome by generating several independent models and then averaging them [29].

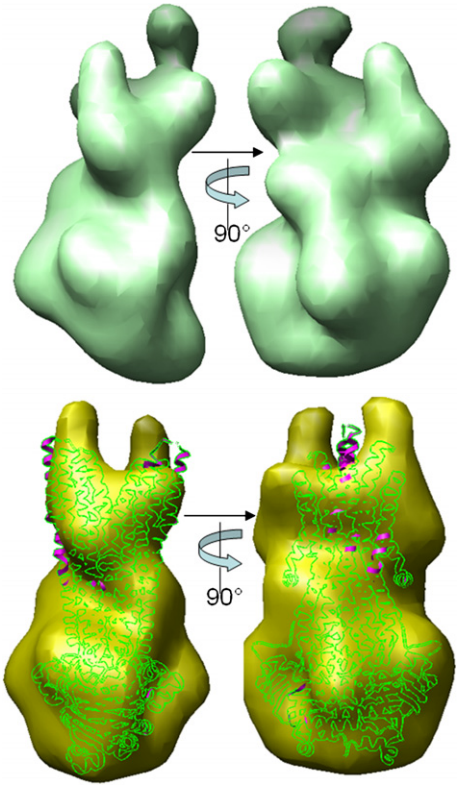

Fig. 2. Orthogonal views of the ab initio-generated low resolution 3D density distribution calculated using the SAXS profile for ABCB1 and applying no symmetry (top, green surface) or C2 symmetry (bottom, yellow semi-transparent surface). The latter data is compared with an optimised fit with the bacterial ABC transporter Sav1866 (ribbon trace). Regions of the Sav1866 structure that lie within the calculated density distribution are indicated by the green outline, whilst regions lying outside the boundaries are highlighted in purple.

3.3. ABCB1 structure after correction using the SAXS data

EM data has phase information but the amplitude information is distorted. Hence we corrected the distortions using the well defined amplitude information from SAXS of ABCB1. Fig. 3 shows a single ABCB1 molecule within the ~8 Å-resolution map after such correction. Compared to the previously published map [6], the SAXS-corrected map showed better definition of peripheral features of the EM map, e.g. the extracellular loop regions and the NBDs. Two features that were previously fitted as short alpha helical elements on the extracellular surface [6] are consistent with extensions of transmembrane helices, as observed for the Sav1866 structure.

Fitting the Sav1866 structure, initially manually and then automatically with the *Chimera* 'fit to map' routine [31], yielded a good correspondence between the Sav1866 structure (backbone atoms) and the ABCB1 map (Fig. 3, right hand panel). The average density value of the map at the locations of the 4624 backbone atoms of Sav1866 was 0.82σ above the mean. In comparison, other ABC proteins with less homology to ABCB1 yielded poorer fits. The 4296 backbone atoms of BtuCD [13], and the 5180 backbone atoms of ModABC [11], have values of 0.64 and 0.65σ above the mean (respectively). As previously noted [6], the ABCB1 map shows an approximation to non-crystallographic (NCS) two-fold symmetry.

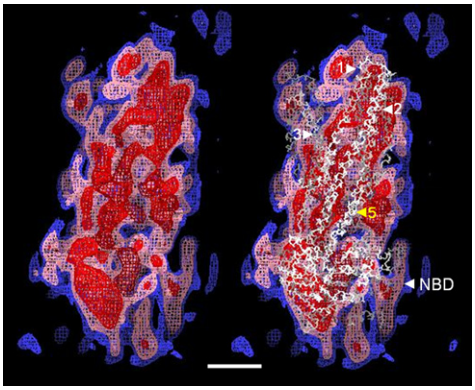

Fig. 3. ABCB1 map at ~8 Å resolution after global correction of experimental amplitudes with the SAXS profile shown in Fig. 1. The panels show the unsymmetrised map using blue, pink and red netting to represent density at 1, 2 and 4σ above the mean level, respectively. The panel on the right shows the bacterial homologue, Sav1866 fitted to the map (white Cα trace). Sav1866 transmembrane domain helices 1, 2, 3 (and 5 from the opposite monomer) are indicated. The scale bar corresponds to 20 Å.

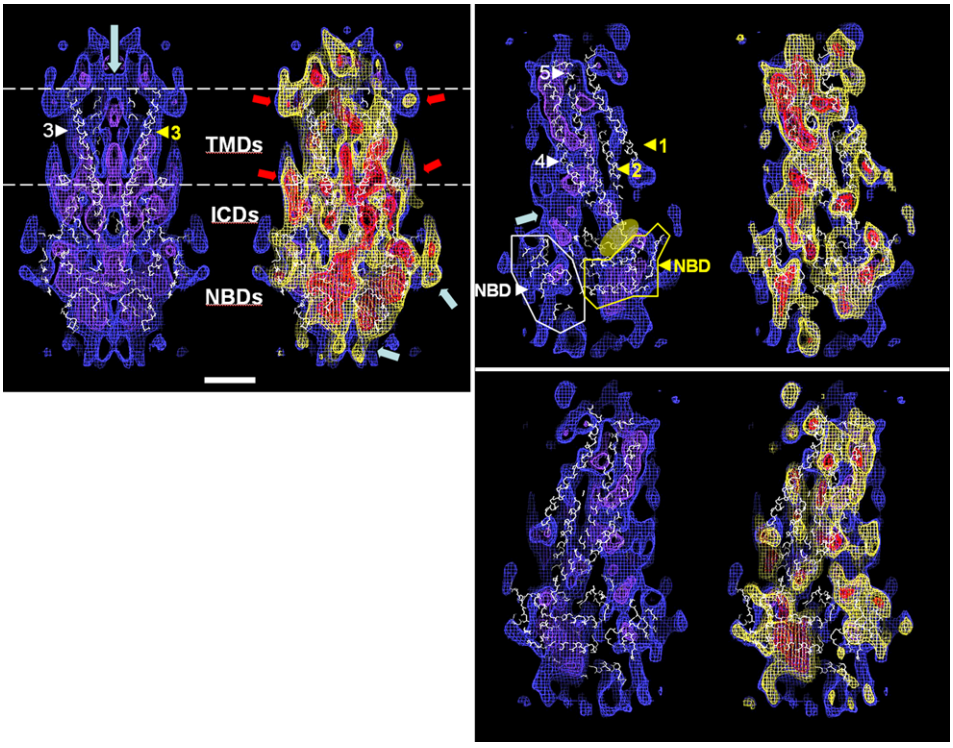

Fig. 4. Map sections (1 nm thick) parallel to the pseudo-NCS axis. The left-hand sections are after application of two-fold rotational symmetry about the (vertical) NCS axis, with blue netting at 2σ above the mean density and purple netting at 6σ. The right-hand sections in each panel show the corresponding unsymmetrised map superimposed, using yellow and red netting to represent density at 2 and 6σ above the mean level, respectively. In each case, the bacterial homologue, Sav1866 is fitted to the map (white Cα trace), and the TM helices numbered. Sections equidistant from the C2 symmetry axis through the rear, and front of the map are shown in the panels on the right. The scale bar corresponds to 20 Å.

A Fourier shell correlation (FSC) analysis of the unsymmetrised map versus a 180°-rotated version of it was carried out, and a FSC = 0.5 value was passed at a resolution of about 23 Å. In comparison with other membrane proteins that have arisen by gene duplication [35] this seemed reasonable. For example, the L and M subunits of the *Rhodopseudomonas sphaeroides* photosynthetic reaction centre (sequence identity ~30%) display an overall C2 symmetry to about 21 Å [36] whilst the A and B subunits of cyanobacterial photosystem I (sequence identity ~44%) display C2 symmetry to about 12 Å [37]. Consequently, we applied real space averaging to facilitate comparison with the Sav1866 structure [9]. Features in the ABCB1 map that are not related by symmetry will be smeared out, but the exercise allowed a comparison of the overall 'footprint' of ABCB1 versus the equivalent Sav1866 regions.

A section along the pseudo-C2 symmetry axis is shown in Fig. 4. The NBD region at the bottom shows two heart-shaped lobes of density that match the expected NBD structure. Additional features may be due to the linker region between NBD1 and TMD2 and/or the C-terminus of ABCB1 (blue arrows). The centre of the TMD region shows a 'V' shaped profile with a good match between cylindrical densities and Sav1866 TM helices 3. A central density is not occupied by the fitted Sav1866 model (blue arrow, see also Fig. 4). The position of the membrane-spanning region in Sav1866 is indicated by the dashed lines. Interestingly, densities protrude outwards in the ABCB1 map at the expected lipid bilayer boundaries (red arrows). In Sav1866 [9], an N-terminal amphipathic helix is in a position consistent with it being embedded into the cytoplasmic surface of the membrane and therefore adds significant density in this boundary region. Two sections taken equidistant from the C2 symmetry axis are also displayed in Fig. 4. The discrimination between the two halves of the ABCB1 molecule is clear from these sections, with a leftwards tilt to the TMD in the rearmost section and to the right in the front section (lower panel). The position of the intracytoplasmic loop (ICL) between helices 4 and 5 in Sav1866 that makes contact with the opposing NBD is indicated by the yellow ellipse in the upper panel. The ABCB1 map shows density in this region. A region not matched by the Sav1866 model in the ICL region is indicated by the blue arrows. Fig. 5 shows three sections from the ABCB1 map taken perpendicular to the C2 symmetry axis and representing the TMD, ICL and NBD regions. For each section, the unsymmetrised map and symmetrised maps are again compared. The map in the NBD region is consistent with a closed dimer configuration, as expected for nucleotide-bound protein [2,38,39]. The overall footprint of Sav1866 in this region is similar to the density in the ABCB1 map, and the expected position of the adenine ring of the AMP–PNP molecules in Sav1866 is indicated by the red arrows. In Sav1866, the cytoplasmic loop between TM helices 4 and 5 forms contacts with the opposing NBD [9]. As discussed above, there is density present in the ABCB1 map in the expected position of this loop (yellow ellipses). In the ICL region, the footprint of Sav1866 again matches the ABCB1 map and any asymmetry in this region (arrows) is likely to arise from the linker region connecting NBD1 to TMD2.

In the membrane-spanning region, most of the Sav1866 helices map into available density in the unsymmetrised ABCB1

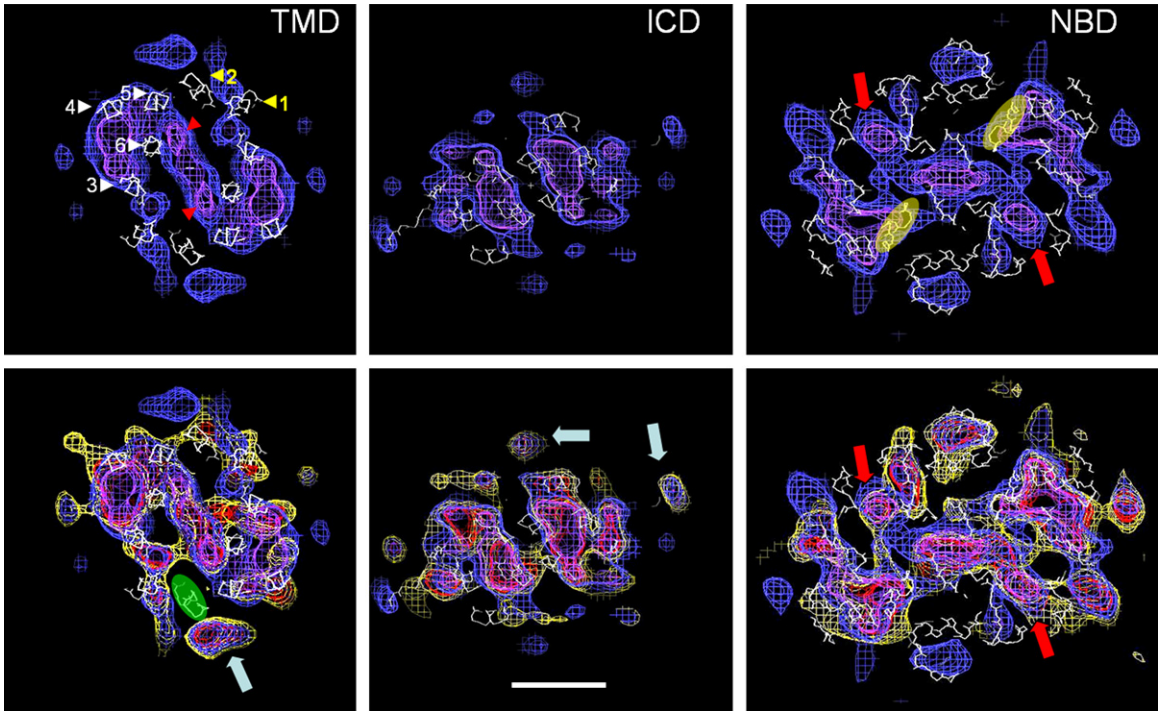

Fig. 5. Sections (1 nm thick) perpendicular to the pseudo-NCS axis.The upper panels show the map after application of two-fold rotational symmetry and the lower panels show the corresponding section of the unsymmetrised map superimposed, with netting as in Fig. 3. In each case, the bacterial homologue, Sav1866 is fitted to the map (white Cα trace). Slices through the transmembrane, intracytoplasmic loop and nucleotide binding domains are shown left, centre and right, respectively. Sav1866 transmembrane domain helices are indicated in the top left panel. The scale bar corresponds to 20 Å.

map, with the exception of the two transmembrane helices 6, and one of the two transmembrane helices 2 which falls in a gap on the periphery of the ABCB1 map (green ellipse). As previously reported [6], peripheral densities are somewhat asymmetrical (blue arrow), and a gap on one side of the protein is closed on the other side. At the centre of the ABCB1 map, the two transmembrane helices 6 of Sav1866 would have to move about 5 Å inwards to give a good fit. Data obtained previously by cross-linking of inserted cysteine residues suggests that helices 6 and 12 are indeed close together in ABCB1 [40,41]. The same technique also identifies a close association of helices 2 and 11 and 5 and 8 in ABCB1 [42,43], consistent with the arrangement of these helices (2 and 5) in the Sav1866 homodimer [9].

A homology model for ABCB1 based on the bacterial Sav1866 structure has already been published [44]. Eukaryotic NBD structures will be similar to their bacterial counterparts [38,45–47], but for the TMD regions, homology at the level of primary through to tertiary structure could be weak. The six bacterial ABC proteins yielding high resolution structural information, show surprising TMD plasticity (three distinct folds are evident) [9–16]. Moreover, recent data show that two identical TMDs can adopt slightly different structures when a periplasmic protein is bound [12]. If such plasticity and asymmetry is at work in eukaryotic ABC proteins, then modelling the crucial TMD regions will be challenging. The work presented here, however, demonstrates that modelling of eukaryotic transporters on the basis of bacterial counterparts is likely to be productive, especially where experimental validation of models of eukaryotic ABC proteins is possible using a combination of low to medium resolution structural methods such as SAXS and EM.

Acknowledgements: We thank Drs. Ian Kerr (University of Nottingham), Megan O'Mara (University of British Columbia), Kenneth Linton (MRC Clinical Sciences Centre, Hammersmith) and Clair Baldock (University of Manchester) for useful discussions, encouragement and advice This work is funded by Project Grants from Cancer Research UK (C362/A5806) and the Medical Research Council UK (G040063).

Appendix A. Supplementary material

Supplementary data associated with this article can be found, in the online version, at doi:10.1016/j.febslet.2008.07.022.

References

[1] Higgins, C.F. (2007) Multiple molecular mechanisms for multidrug resistance transporters. Nature 446, 749–757.
[2] Callaghan, R., Ford, R.C. and Kerr, I.D. (2006) The translocation mechanism of P-glycoprotein. FEBS Lett. 580, 1056–1063.
[3] Rosenberg, M.F., Callaghan, R., Ford, R.C. and Higgins, C.F. (1997) Structure of the multidrug resistance P-glycoprotein to 2.5 nm resolution determined by electron microscopy and image analysis. J. Biol. Chem. 272, 10685–10694.
[4] Rosenberg, M.F., Velarde, G., Ford, R.C., Martin, C., Berridge, G., Kerr, I.D., Callaghan, R., Schmidlin, A., Wooding, C., Linton, K.J. and Higgins, C.F. (2001) Repacking of the transmembrane domains of P-glycoprotein during the transport ATPase cycle. EMBO J. 20, 5615–5625.

[5] Rosenberg, M.F., Mao, Q., Holzenburg, A., Ford, R.C., Deeley, R.G. and Cole, S.P. (2001) The structure of the multidrug resistance protein 1 (MRP1/ABCC1). Crystallization and single-particle analysis. J. Biol. Chem. 276, 16076–16082.
[6] Rosenberg, M.F., Callaghan, R., Modok, S., Higgins, C.F. and Ford, R.C. (2005) Three-dimensional structure of P-glycoprotein: the transmembrane regions adopt an asymmetric configuration in the nucleotide-bound state. J. Biol. Chem. 280, 2857–2862.
[7] Rosenberg, M.F., Kamis, A.B., Callaghan, R., Higgins, C.F. and Ford, R.C. (2003) Three-dimensional structures of the mammalian multidrug resistance P-glycoprotein demonstrate major conformational changes in the transmembrane domains upon nucleotide binding. J. Biol. Chem. 278, 8294–8299.
[8] Ford, R.C. and Holzenburg, A. (2008) Electron crystallography of biomolecules: mysterious membranes and missing cones. Trends Biochem. Sci. 33, 38–43.
[9] Dawson, R.J. and Locher, K.P. (2006) Structure of a bacterial multidrug ABC transporter. Nature 443, 180–185.
[10] Dawson, R.J. and Locher, K.P. (2007) Structure of the multidrug ABC transporter Sav1866 from *Staphylococcus aureus* in complex with AMP–PNP. FEBS Lett. 581, 935–938.
[11] Hollenstein, K., Frei, D.C. and Locher, K.P. (2007) Structure of an ABC transporter in complex with its binding protein. Nature 446, 213–216.
[12] Hvorup, R.N., Goetz, B.A., Niederer, M., Hollenstein, K., Perozo, E. and Locher, K.P. (2007) Asymmetry in the structure of the ABC transporter-binding protein complex BtuCD–BtuF. Science 317, 1387–1390.
[13] Locher, K.P., Lee, A.T. and Rees, D.C. (2002) The *E. coli* BtuCD structure: a framework for ABC transporter architecture and mechanism. Science 296, 1091–1098.
[14] Pinkett, H.W., Lee, A.T., Lum, P., Locher, K.P. and Rees, D.C. (2007) An inward-facing conformation of a putative metal-chelate-type ABC transporter. Science 315, 373–377.
[15] Oldham, M.L., Khare, D., Quiocho, F.A., Davidson, A.L. and Chen, J. (2007) Crystal structure of a catalytic intermediate of the maltose transporter. Nature 450, 515–521.
[16] Ward, A., Reyes, C.L., Yu, J., Roth, C.B. and Chang, G. (2007) Flexibility in the ABC transporter MsbA: alternating access with a twist. Proc. Natl. Acad. Sci. USA 104, 19005–19010.
[17] Rothnie, A., Storm, J., Campbell, J., Linton, K.J., Kerr, I.D. and Callaghan, R. (2004) The topography of transmembrane segment six is altered during the catalytic cycle of P-glycoprotein. J. Biol. Chem. 279, 34913–34921.
[18] Rothnie, A., Storm, J., McMahon, R., Taylor, A., Kerr, I.D. and Callaghan, R. (2005) The coupling mechanism of P-glycoprotein involves residue L339 in the sixth membrane spanning segment. FEBS Lett. 579, 3984–3990.
[19] Storm, J., O'Mara M, L., Crowley, E.H., Peall, J., Tieleman, D.P., Kerr, I.D. and Callaghan, R. (2007) Residue G346 in transmembrane segment six is involved in inter-domain communication in P-glycoprotein. Biochemistry 46, 9899–9910.
[20] Hamada, D., Higurashi, T., Mayanagi, K., Miyata, T., Fukui, T., Iida, T., Honda, T. and Yanagihara, I. (2007) Tetrameric structure of thermostable direct hemolysin from vibrio parahaemolyticus revealed by ultracentrifugation, small-angle X-ray scattering and electron microscopy. J. Mol. Biol. 365, 187–195.
[21] Vestergaard, B., Sanyal, S., Roessle, M., Mora, L., Buckingham, R.H., Kastrup, J.S., Gajhede, M., Svergun, D.I. and Ehrenberg, M. (2005) The SAXS solution structure of RF1 differs from its crystal structure and is similar to its ribosome bound cryo-EM structure. Mol. Cell 20, 929–938.
[22] Saad, A., Ludtke, S.J., Jakana, J., Rixon, F.J., Tsuruta, H. and Chiu, W. (2001) Fourier amplitude decay of electron cryomicroscopic images of single particles and effects on structure determination. J. Struct. Biol. 133, 32–42.
[23] Amos, L.A., Henderson, R. and Unwin, P.N. (1982) Three-dimensional structure determination by electron microscopy of two-dimensional crystals. Prog. Biophys. Mol. Biol. 39, 183–231.
[24] Rice, W.J., Young, H.S., Martin, D.W., Sachs, J.R. and Stokes, D.L. (2001) Structure of Na+, K+-ATPase at 11-Å resolution: comparison with Ca^{2+}-ATPase in E1 and E2 states. Biophys. J. 80, 2187–2197.
[25] Tsuruta, H., Reddy, V.S., Wikoff, W.R. and Johnson, J.E. (1998) Imaging RNA and dynamic protein segments with low-resolution virus crystallography: experimental design, data processing and implications of electron density maps. J. Mol. Biol. 284, 1439–1452.
[26] Kilaas, R., Marks, L.D. and Own, C.S. (2005) EDM 1.0: electron direct methods. Ultramicroscopy 102, 233–237.
[27] Taylor, A.M., Storm, J., Soceneantu, L., Linton, K.J., Gabriel, M., Martin, C., Woodhouse, J., Blott, E., Higgins, C.F. and Callaghan, R. (2001) Detailed characterization of cysteine-less P-glycoprotein reveals subtle pharmacological differences in function from wild-type protein. Br. J. Pharmacol. 134, 1609–16018.
[28] Baldock, C., Siegler, V., Bax, D.V., Cain, S.A., Mellody, K.T., Marson, A., Haston, J.L., Berry, R., Wang, M.C., Grossmann, J.G., Roessle, M., Kielty, C.M. and Wess, T.J. (2006) Nanostructure of fibrillin-1 reveals compact conformation of EGF arrays and mechanism for extensibility. Proc. Natl. Acad. Sci. USA 103, 11922–11927.
[29] Svergun, D.I., Petoukhov, M.V. and Koch, M.H. (2001) Determination of domain structure of proteins from X-ray solution scattering. Biophys. J. 80, 2946–2953.
[30] Volkov, V.V. and Svergun, D.I. (2003) Uniqueness of ab initio shape determination in small-angle scattering. J. Appl. Crystallogr. 36, 860–864.
[31] Goddard, T.D., Huang, C.C. and Ferrin, T.E. (2007) Visualizing density maps with UCSF Chimera. J. Struct. Biol. 157, 281–287.
[32] Frank, J., Radermacher, M., Penczek, P., Zhu, J., Li, Y., Ladjadj, M. and Leith, A. (1996) SPIDER and WEB: processing and visualization of images in 3D electron microscopy and related fields. J. Struct. Biol. 116, 190–199.
[33] Ludtke, S.J., Baldwin, P.R. and Chiu, W. (1999) EMAN: semiautomated software for high-resolution single-particle reconstructions. J. Struct. Biol. 128, 82–97.
[34] Tang, G., Peng, L., Baldwin, P.R., Mann, D.S., Jiang, W., Rees, I. and Ludtke, S.J. (2007) EMAN2: an extensible image processing suite for electron microscopy. J. Struct. Biol. 157, 38–46.
[35] Stenham, D.R., Campbell, J.D., Sansom, M.S., Higgins, C.F., Kerr, I.D. and Linton, K.J. (2003) An atomic detail model for the human ATP binding cassette transporter P-glycoprotein derived from disulfide cross-linking and homology modeling. FASEB J. 17, 2287–2289.
[36] Allen, J.P., Feher, G., Yeates, T.O., Rees, D.C., Deisenhofer, J., Michel, H. and Huber, R. (1986) Structural homology of reaction centers from *Rhodopseudomonas sphaeroides* and *Rhodopseudomonas viridis* as determined by X-ray diffraction. Proc. Natl. Acad. Sci. USA 83, 8589–8593.
[37] Schubert, W.D., Klukas, O., Krauss, N., Saenger, W., Fromme, P. and Witt, H.T. (1997) Photosystem I of *Synechococcus elongatus* at 4 Å resolution: comprehensive structure analysis. J. Mol. Biol. 272, 741–769.
[38] Kerr, I.D. (2002) Structure and association of ATP-binding cassette transporter nucleotide-binding domains. Biochim. Biophys. Acta 1561, 47–64.
[39] Locher, K.P. (2004) Structure and mechanism of ABC transporters. Curr. Opin. Struct. Biol. 14, 426–431.
[40] Loo, T.W. and Clarke, D.M. (2000) The packing of the transmembrane segments of human multidrug resistance P-glycoprotein is revealed by disulfide cross-linking analysis. J. Biol. Chem. 275, 5253–5256.
[41] Loo, T.W. and Clarke, D.M. (1999) Determining the structure and mechanism of the human multidrug resistance P-glycoprotein using cysteine-scanning mutagenesis and thiol-modification techniques. Biochim. Biophys. Acta 1461, 315–325.
[42] Loo, T.W., Bartlett, M.C. and Clarke, D.M. (2004) Val133 and Cys137 in transmembrane segment 2 are close to Arg935 and Gly939 in transmembrane segment 11 of human P-glycoprotein. J. Biol. Chem. 279, 18232–18238.
[43] Loo, T.W., Bartlett, M.C. and Clarke, D.M. (2004) Disulfide cross-linking analysis shows that transmembrane segments 5 and 8 of human P-glycoprotein are close together on the cytoplasmic side of the membrane. J. Biol. Chem. 279, 7692–7697.
[44] O'Mara, M.L. and Tieleman, D.P. (2007) P-glycoprotein models of the apo and ATP-bound states based on homology with Sav1866 and MalK. FEBS Lett. 581, 4217–4222.
[45] Gaudet, R. and Wiley, D.C. (2001) Structure of the ABC ATPase domain of human TAP1, the transporter associated with antigen processing. EMBO J. 20, 4964–4972.

[46] Ramaen, O., Leulliot, N., Sizun, C., Ulryck, N., Pamlard, O., Lallemand, J.Y., Tilbeurgh, H. and Jacquet, E. (2006) Structure of the human multidrug resistance protein 1 nucleotide binding domain 1 bound to Mg^{2+}/ATP reveals a non-productive catalytic site. J. Mol. Biol. 359, 940–949.
[47] Lewis, H.A., Buchanan, S.G., Burley, S.K., Conners, K., Dickey, M., Dorwart, M., Fowler, R., Gao, X., Guggino, W.B., Hendrickson, K.W., Hunt, J.F., Kearins, M.C., Lorimer, D., Maloney, P.C., Post, K.W., Rajashankar, K.R., Rutter, M.E., Sauder, J.M., Shriver, S., Thibodeau, P.H., Thomas, P.J., Zhang, M., Zhao, X. and Emtage, S. (2004) Structure of nucleotide-binding domain 1 of the cystic fibrosis transmembrane conductance regulator. EMBO J. 23, 282–293.